optica

Photonic materials for interstellar solar sailing

Artur R. Davoyan,[1,*] Jeremy N. Munday,[2] Nelson Tabiryan,[3] Grover A. Swartzlander Jr.,[4] and Les Johnson[5]

[1]Department of Mechanical and Aerospace Engineering, University of California, Los Angeles, 420 Westwood Plaza, Los Angeles, California 90095, USA
[2]Department of Electrical and Computer Engineering, University of California, Davis, One Shields Avenue, Kemper Hall Davis, California 95616, USA
[3]BEAM Engineering for Advanced Measurements Co., 1300 Lee Road, Orlando, Florida 32810, USA
[4]Chester F. Carlson Center for Imaging Science, Rochester Institute of Technology, 54 Lomb Memorial Drive, Rochester, New York 14623, USA
[5]NASA George C. Marshall Space Flight Center, Huntsville, Alabama 35808, USA
*Corresponding author: davoyan@seas.ucla.edu

Received 7 December 2020; revised 16 March 2021; accepted 28 March 2021 (Doc. ID 417007); published 17 May 2021

Solar sails are of great promise for space exploration, affording missions that push the limits of the possible. They enable a variety of novel science missions ranging from ultrafast interstellar travel to imaging the poles of the sun—missions that are beyond the reach of current propulsion technology. Here, we describe requirements and challenges associated with optical materials and photonic designs facing the next generation of solar sails. A technology development roadmap is outlined to guide researchers in pioneering the space faring future.

https://doi.org/10.1364/OPTICA.417007

1. INTRODUCTION

Sixty years of space exploration have led to breakthrough discoveries in a broad range of disciplines, from cosmology to particle physics to plasma physics to geology. Presently, missions to planets and other bodies in the solar system further our understanding of planetary birth and shed light on the origins of life. Nonetheless, a number of envisioned space missions are beyond the reach of current propulsion technology, including such missions as fast-transit probes to interstellar medium [1–5] and solar polar imaging [6–10]. Indeed, only two probes, Voyager 1 and Voyager 2, launched in 1977, have just recently crossed the heliopause (the boundary separating our planetary system from the interstellar medium), in 2012 and 2018, respectively (see Fig. 1) [11–13]. It took Voyager 1 nearly 35 years of flight at 17 km/s to reach the interstellar region [12]. Clearly, a more accessible and sustainable way of exploring distant objects of our solar system and of interstellar medium are needed.

Solar polar imaging is another example of a mission that is beyond the reach of current propulsion technology [6–10]: due to a limited fuel budget of current spacecraft it is extremely difficult to leave the orbital plane of the planets (the ecliptic) to travel across the poles of the sun (see Sec. 2). The recently launched Parker Solar Probe [14] utilized multiple gravity assists from Venus to become the closest manmade object to examine the sun, yet reaching only a modest 3.4° inclination above the ecliptic. Whereas Voyager and Parker Solar Probe missions push the boundaries of space exploration, further advances in spacecraft design and propulsion are necessary to enable a more efficient pathway for space travel.

Solar sails, unlike regular chemical and electrical rockets, make use of solar radiation pressure for propulsion and offer a conceptually different approach to space exploration [15–24]. Without a need to carry onboard propellant or heavy engines, even minute radiation pressure forces may be continuously harnessed to accelerate lightweight solar sail spacecraft to unprecedented velocities and destinations [16–22]. One of the key performance metrics for solar sailing is the characteristic acceleration—radiation pressure force per solar sail spacecraft mass, $a_0 = 2\frac{S_{1\,\mathrm{AU}}}{c}$ (A/m) [20], here $S_{1\,\mathrm{AU}} \simeq 1{,}360\ \mathrm{W/m^2}$ = standard air mass zero (AM0) solar flux at Earth, A = sail area, m = overall solar sail spacecraft mass, and c = speed of light (normal incidence and unity reflectance are assumed). Lightweight solar sails, that is, with a large A/m ratio, have a potential to open a new chapter for space exploration with a particular promise for interstellar flight. Hence, it was suggested that by performing a slingshot (the so-called powered gravity assist or Oberth maneuver) in close proximity to the sun [Fig. 1(a)], lightweight solar sails may be accelerated to unprecedented velocities [16–19] (see Sec. 2 for a detailed discussion on basic principles of solar sailing and Oberth maneuver). In Fig. 1(b), we plot an expected solar sail velocity versus area-to-mass ratio, A/m, after a powered slingshot maneuver with perihelion distance [i.e., closest distance to the sun, see also Fig. 1(a) and Sec. 2] [17,18,22]. Velocities well in excess of 20 AU/year (i.e., >100 km/s) are possible, that is, more than five times that of Voyager 1. We note that whereas laser propulsion can potentially accelerate a spacecraft to even higher, near relativistic, velocities [25–27], solar sails do not require capital infrastructure associated with large aperture high power laser arrays [27] and can carry kilograms of useful load. The velocities that may be achieved by solar sails exceed those of other

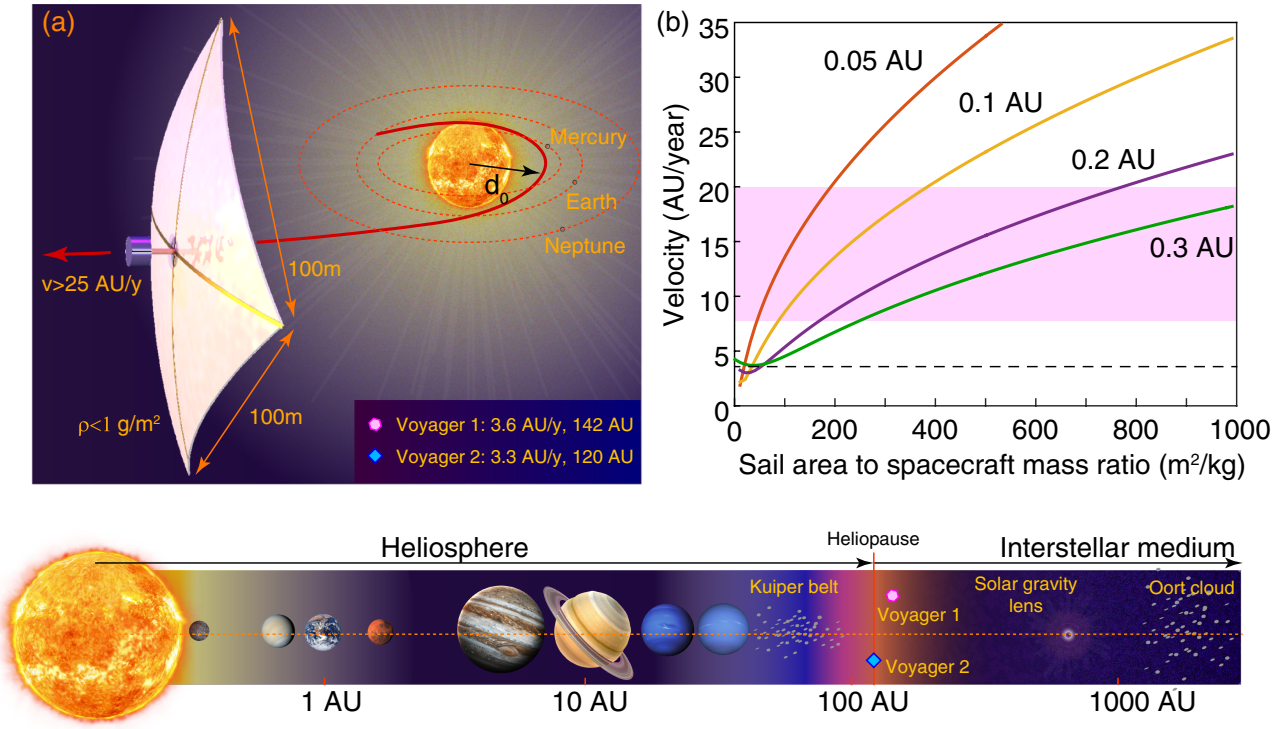

Fig. 1. Solar sails for interstellar space missions. (a) Conceptual illustration of a solar sail interstellar probe. By making use of a powered gravity assist in close proximity to the sun, a sail-craft may be propelled to over 25 AU/year. Key solar sail parameters, including size and aerial density are shown. Inset shows velocity and current distance from the sun for Voyagers 1 and 2—the only two probes that have left the heliosphere. (b) An estimate of the solar sail velocity with sail-area-to-spacecraft-mass ratio for different perihelion distances. Shaded region highlights the span of velocities for other proposed propulsion technologies, including solar thermal, nuclear electric, and chemical rockets with several gravity assist maneuvers. Dashed line shows the velocity of Voyager 1 for comparison. The inset below panels (a) and (b) illustrates the scales in the solar system, shows the positions of Voyagers 1 and 2 and the heliosphere boundary. A solar sail probe discussed in this perspective would be able to reach interstellar space in less than 5 years and solar gravity lens in less than 20 years.

proposed propulsion concepts, including solar thermal [28], large chemical rockets utilizing solar and Jovian slingshot maneuvers [29–31], and nuclear electric propulsion [5,29,32]. With such high velocities, solar sailing may pave the way to a new era of solar imaging, deep space and interstellar exploration. Regular space missions to Pluto [33] within a year, reaching the heliopause and overtaking Voyager 1 [12,13] in less than 5 years, placing exoplanet observatories at the solar gravitational lensing point at ∼550 AU [22] and potentially exploring Planet Nine [34] (400 AU–800 AU) within 10–20 years of travel all become feasible.

Demonstrations of solar sailing over the last decade proved unique capabilities of this technology for near-Earth and inner solar system operations (Fig. 2). Most notable missions include IKAROS (interplanetary kite-craft accelerated by radiation of the sun, launched in 2010 [35,36] —the first interplanetary solar sail demonstration mission; NanoSail-D2 (2011), LightSail 1 (2015), and LightSail 2 (2019) [37,38]—cube satellite based solar sail technology demonstration missions; near-Earth asteroid scout—the first science mission to perform reconnaissance of a small asteroid (2021 planned launch date) [39]; and Solar Cruiser —the first heliophysics mission (2025 planned launch date) that will demonstrate the capabilities needed for a solar sail to observe the sun from vantage points not accessible before [40,41], including imaging of the solar poles. Unlike these early-stage missions, journeys to interstellar space present significant scientific and engineering complexities, which challenge the frontiers of current technology. Indeed, to propel just a 10 kg payload carrying instruments, deployment mechanisms, controls, and communications to 25 AU/year, a 100 × 100 m^2 sail with less than 1 g/m^2 aerial density, that is, less than 1 μm thick, would have to perform a powered flyby maneuver as close as ∼20 solar radii from the sun's surface [Figs. 1(a) and 1(b)] [19–22]. While Solar Parker Probe will fly as close as 9 solar radii from the sun [14], stringent requirements on sail optical properties, its mass and area pose a significant challenge and require a dedicated research and development effort. Solar sail-based interstellar precursor missions would need to push the boundaries of materials science, photonic design, structural engineering, controls, and communications.

In this perspective, we outline challenges and key design criteria facing future solar sail interstellar missions and missions that benefit from a close approach to the sun, with a particular focus on sail optical properties and photonic designs. Specifically, we begin our discussion with Sec. 2 that provides a brief survey of conventional propulsion technologies and their limitations. Sec. 2 also highlights basic principles of light sailing and solar sailing, in particular. We conclude the section with a discussion of key figures of merit for interstellar solar sailing.

We then provide an overview of photonic materials needed for such future solar sail missions in Sec. 3. Efficient sail propulsion necessitates materials that are lightweight, have high reflectivity, low solar absorptivity, and are capable of withstanding high temperatures. With radiative cooling being the sole mechanism for

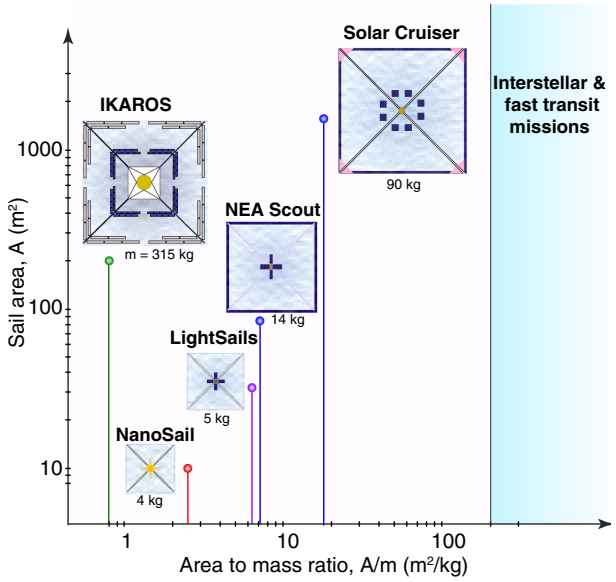

Fig. 2. Illustration of solar sail missions flown and planned arranged by their area, A, and sail area to spacecraft mass ratio, A/m. For ultrafast solar system exploration and interstellar travel solar sails with $A/\mathrm{m} \geq 200\ \mathrm{m}^2/\mathrm{kg}$ are needed.

thermal regulation, in Sec. 3 we highlight the importance of photonic design to balance sunlight absorption and heat load caused by the solar plasma on one hand and thermal emissivity on the other. We show that with a reasonable design, sail operation temperature may be sustained at less than 1000 K (for comparison, the annealing point of fused silica is ∼1420 K). We further discuss possible nanostructures and materials that can provide high propulsive force at this temperature range.

A spacecraft requires not only propulsion, but also attitude and navigational control by use of force and torque. With sunlight as a propellant, active and passive control of the radiation pressure force and its distribution over the sail structure becomes increasingly important. In Sec. 4 we show that by making use of nanophotonic design and dispersion engineering novel opportunities for tailoring propulsive force and sail attitude emerge. Recent advances in diffraction gratings and metasurfaces enable passive control of angular distribution of the radiation pressure forces beyond capabilities of regular mirrors. For active control, liquid crystals provide an attractive mechanism for active electro-optical materials with adjustable optical properties [24].

Extreme environmental conditions (Sec. 5) that might be encountered by a solar sail interstellar probe, particularly during its active propulsion phase, pose another design constraint. Hence, a sail on its small perihelion approach (≥20 solar radii) will have to sustain interaction with solar corona and high energy photon and elementary particle fluxes. In addition, the large surface area of the sail ($>10{,}000\ \mathrm{m}^2$) increases the probability of collision with dust particulates orbiting the sun at very high velocities (100 s of km/s) and micrometeorites over the course of active propulsion within the inner solar system. Understanding the solar and space environment over the active phase of sail propulsion is therefore critical to minimizing materials degradation.

In Sec. 6 we make a very brief overview of other challenges that may face interstellar solar sailing. Finally, Sec. 7 provides a comparison between solar sailing and laser sailing.

In this perspective, we review the aforementioned issues and show that the challenges of future solar sail interstellar probe missions can be met with a development of novel nanophotonic materials. We believe that further progress in photonics and materials science will enable a new generation of solar sails that will transform deep space exploration in the near future.

2. INTERSTELLAR SOLAR SAILING PROPULSION: BACKGROUND

We begin our discussion with an overview of conventional chemical and electrical propulsion technologies, and an outline of fundamental advantages solar sails may offer.

Chemical and electric engines are the two major means of propulsion in space. Chemical rockets are the backbone of manned and interplanetary missions, whereas electric engines, such as plasma and electrospray thrusters, are used for station keeping and efficient orbital maneuvering [42,43]. While these propulsion methods are conceptually different, they are based on the same fundamental principle: producing thrust by expelling fuel *carried on board* a spacecraft [42,43]. The amount and the velocity of fuel expulsion directly determine the range of velocities and destinations a spacecraft may reach. As a measure of spacecraft capability for acceleration, a velocity gain parameter, Δv, governed by Tsiolkovsky's rocket equation, is introduced [42]:

$$\Delta v = v_{\mathrm{ex}} \ln\left(\frac{m_0}{m_f}\right), \tag{1}$$

where v_{ex} is the exhaust velocity, i.e., velocity at which propellant is expelled out of the rocket, m_0 is the initial mass of the spacecraft including the on-board fuel carried, and m_f is the final mass of the spacecraft after fuel is expended to reach a desired velocity. Evidently, the higher is the fuel exhaust velocity, v_{ex}, the more velocity gain, Δv, a spacecraft may obtain. For chemical rocket engines, the exhaust velocity is limited by the average kinetic energy of its reacting species and $v_{\mathrm{ex}} \leq 5$ km/s. Electric engines can yield more than an order of magnitude higher fuel exhaust velocity, however, at a cost of smaller thrust and, therefore, much longer acceleration time [42]. For instance, the recently launched Dawn spacecraft has $v_{\mathrm{ex}} \simeq 31$ km/s and provides 90 mN thrust [44]. While Dawn set a record velocity gain of $\Delta v \simeq 11$ km/s, it took ∼4 years to reach Vesta, one of the largest objects in the asteroid belt. The fundamental limitation of conventional propulsion for fast solar system exploration and interstellar flight becomes readily evident from the rocket equation Eq. (1). For instance, to achieve 20 AU/year (≃95 km/s) cruise velocity for interstellar flight (cf. with Voyager 1 at ≃3.6 AU/year or 17 km/s, see also Fig. 1), a chemical rocket with $v_{\mathrm{ex}} = 5$ km/s would need $m_f \geq m_0 \times 10^{-6}$. That is, to propel just a 10 kg spacecraft $\gg 10^4$ ton of fuel would be needed! For comparison, the mass of Falcon heavy rocket is ∼1400 tons. Similarly, to perform inclination change maneuvers such as leaving the plane of ecliptic also requires a very high velocity gain [40,41]: $\Delta v = 2v \sin(\psi/2)$ for a change of a plane of circular orbit by an angle ψ by a chemical rocket (here v is the orbital velocity; e.g., $v = 29.78$ km/s is Earth's orbital velocity about the sun). A simple calculation shows that changing an orbital plane of a spacecraft by just 60 deg. would require a velocity gain $\Delta v = v$, which by far exceeds the capability of any of current spacecraft. Interplanetary plane change maneuvers at present are accomplished only with the use of gravity assists, which add complexity to

mission planning and significantly limit the range of possible destinations. The search for more efficient and advanced propulsion methods is currently an active area of research [28–32].

Solar sails make use of solar radiation pressure, they *do not carry propellant on board*, and as such are not subject to the rocket equation limitations [5,20,41]. The ability to utilize external power sources for propulsion fundamentally differentiates solar sails (and laser sails [26,27], for that matter) from other propulsion techniques. Figure 3(a) illustrates basic principles of solar sail propulsion. For the sake of simplicity, we assume an ideal flat sail model and a plane wavefront of incident solar radiation. Solar sail dynamics is governed by an interplay of solar radiation pressure, $\boldsymbol{F}_p$, and solar gravitational attraction, $\boldsymbol{F}_G$ (gravitational pull by planets can be neglected in the context of interstellar and interplanetary missions). Solar radiation pressure force acting on an idealized flat sail may be found as [19]:

$$\boldsymbol{F}_p = \frac{2r\cos(\theta_i)\hat{\boldsymbol{n}} + \alpha\hat{\boldsymbol{d}}}{c} SA, \tag{2}$$

where $\cos(\theta_i) = \hat{\boldsymbol{n}}\hat{\boldsymbol{d}}$ defines the angle of incidence, $\hat{\boldsymbol{d}}$ is the radial unit vector along the sunlight direction, and $\hat{\boldsymbol{n}}$ is a normal to the sail surface, $S = S_{1\,\mathrm{AU}}(((1\,\mathrm{AU})^2)/d^2)$ is the solar irradiance, d is the radial distance from the center of the sun to the sail, r is the sail reflectivity across the solar spectrum ($r = (1/S_{1\,\mathrm{AU}})\int_0^\infty r_\lambda S_{1\,\mathrm{AU},\lambda}(\lambda)\mathrm{d}\lambda$, here $S_{1\,\mathrm{AU},\lambda}(\lambda)$ is a solar spectral power density, r_λ is spectrally resolved reflectivity), and α is the coefficient of solar absorptivity indicating the fraction of the solar flux absorbed by the sail ($\alpha = (1/S_{1\,\mathrm{AU}})\int_0^\infty \alpha_\lambda S_{1\,\mathrm{AU},\lambda}(\lambda)\mathrm{d}\lambda$, here α_λ is spectrally resolved absorptivity). The equation of motion is then found from Newton's second law [42]:

$$\frac{d^2\boldsymbol{d}}{dt^2} = -\frac{\mu_s}{d^3}\boldsymbol{d} + \frac{2r\hat{\boldsymbol{n}}\hat{\boldsymbol{d}} + \alpha}{c}\frac{(1\,\mathrm{AU})^2}{d^2} S_{1\,\mathrm{AU}}\frac{A}{m}\hat{\boldsymbol{n}}, \tag{3}$$

where $\boldsymbol{d}$ is the radius vector pointing from the center of the sun to the solar sail spacecraft, $d = |\boldsymbol{d}|$, and $\mu_s = GM_s$ is the solar gravitational parameter with G denoting gravitational constant and M_s solar mass, respectively. Note that here we ignore second order corrections, such as gravitational attraction by other celestial bodies and radiation pressure due to thermal emission.

Traditionally solar sails are viewed as slow and cumbersome spacecraft that have a very limited range of applications. Indeed, as the radiation pressure drops as $1/d^2$ with distance from the sun, the propulsive force becomes weaker, which necessitates large structures to gain desired momentum. For example, at Earth orbit the solar radiation pressure creates about 1 mN force per every 100 m^2 of solar sail (*cf.* with Dawn spacecraft having 90 mN thrust [44]. However, as solar sails do not necessitate fuel on board and can propel continuously, light-weight structures (i.e., with large area to mass ratio, A/m) can get to trajectories and vantage points that are beyond the reach of conventional spacecraft, including halo orbits and high inclination orbits [6–10,20,41].

For even closer solar approaches (e.g., within an orbit of Mercury or at <0.3 AU), where radiation pressure becomes even stronger, the advantage of solar sailing becomes even more pronounced. In particular, by performing a powered slingshot maneuver the sail may be put onto fast hyperbolic trajectories that can quickly reach distant planets and interstellar space. Such fast-speed interstellar flight was considered in a number of previous works [19–22] [see also Figs. 1 and 3(b)]. In this case, a

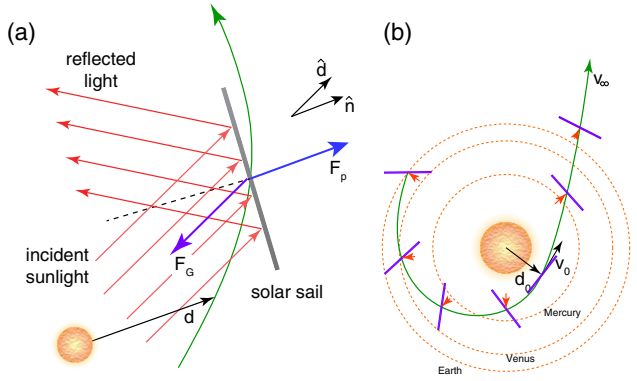

Fig. 3. Principles of solar sail propulsion. (a) A schematic diagram of forces at play for an ideal flat sail: Gravity, F_G, pulls solar sail inward toward the sun, whereas radiation pressure, F_p, creates a force normal to the sail in the outward direction. Balance of the two forces places a sail onto trajectories and orbits beyond the reach of conventional propulsion methods. (b) An illustration of a powered slingshot maneuver placing a solar sail onto a fast-speed hyperbolic trajectory. During the first phase, the solar sail is brought close to the sun, reaching perihelion d_0 at its closest approach; the solar sail velocity at this point is v_0. Once at perihelion, the sail is oriented normally to the sun to perform a powered slingshot. Orientation of the sail during maneuvering is schematically shown. Both panels (a) and (b) are not to scale.

sail originally deployed at an Earth orbit is brought to its closest approach about the sun—perihelion, d_0 [Fig. 3(b)]. This maneuver is performed by gradual *spiraling in*, which is achieved by orienting the sail at an angle to the sunline direction $\hat{\boldsymbol{d}}$ [similarly to the case shown in Fig. 3(a)]. In this case, the tangential component of the radiation pressure force is directed against the velocity vector causing the sail to lose energy and gradually fall toward the sun. Once at perihelion, the sail is oriented perpendicular to the sun to attain a maximum possible propulsive action that puts it onto a hyperbolic escape trajectory Fig. 3(b). This phase is known as a powered slingshot or Oberth maneuver, where gravitational attraction and the radiation pressure interplay to create a strong propulsive force. For a normally incident sunlight ($\theta_i = 0$, $\hat{\boldsymbol{n}} = \hat{\boldsymbol{d}}$), Eq. (3) is substantially simplified:

$$\frac{d^2\boldsymbol{d}}{dt^2} = -\frac{\mu_{\mathrm{eff}}}{d^3}\boldsymbol{d}, \tag{4}$$

where $\mu_{\mathrm{eff}} = \mu_s - (2r+\alpha)\frac{S_{1\,\mathrm{AU}}}{c}(1\,\mathrm{AU})^2\frac{A}{m}$ plays the role of an effective gravitational parameter. Equation (4) is a familiar orbital dynamics equation describing standard Keplerian circular, elliptical, and hyperbolic orbits [42]. In the absence of solar effects (i.e., for $r \to 0$ and $\alpha \to 0$) $\mu \to \mu_s = GM_s$ and Eq. (4) reduces to a conventional orbital dynamics equation about the sun.

Once placed onto a hyperbolic trajectory, the solar sail will asymptotically reach a cruise velocity that may be approximated as [43]:

$$v_\infty \simeq \sqrt{v_0^2 - 2\frac{\mu_{\mathrm{eff}}}{d_0}}, \tag{5}$$

where v_0 and d_0 are velocity and position of the solar sail at the perihelion, respectively, right before the powered slingshot is performed [Fig. 3(b)]. The velocity at the perehelion, v_0, depends on prior phases of the mission (i.e., the way the solar sail is brought from Earth to the perihelion). However, its upper bound may be

approximated as $v_0 \simeq \sqrt{2(\mu_s/d_0)(1\,\mathrm{AU}/(1\,\mathrm{AU}+d_0))}$ (here we assume a Hohmann transfer [43]). For example, for $d_0 = 0.1$ AU perihelion (i.e., three times closer to the sun than Mercury) $v_0 \simeq 127$ km/s. The bound on the maximum cruise velocity that a solar sail may reach is then found as

$$v_\infty \simeq \sqrt{-\frac{2\mu_s}{1\,\mathrm{AU}+d_0} + 2(2r+\alpha)\frac{S_{1\mathrm{AU}}}{c}\frac{(1\,\mathrm{AU})^2}{d_0}\frac{\mathrm{A}}{\mathrm{m}}}. \quad (6)$$

Evidently, the solar sail velocity depends on its optical properties (i.e., solar reflectivity and absorptivity), sail area to total spacecraft mass ratio, A/m, and the perehelion, d_0. Smaller d_0 and higher A/m ratio yield higher cruise velocities. In Fig. 1(b), we plot the sail cruise velocity with area to mass ratio for different perihelion approaches for a perfectly reflecting sail (i.e., $r = 1$ and $\alpha = 0$). Velocities in excess of 20 AU/year, that is, faster than any other near-term propulsion methods under consideration [28–30], can be reached for close perihelion approaches ($d_0 < 0.2$ AU) and high sail area to mass ratios (A/m > 200 m^2/kg). The closest range of solar approaches [i.e., min(d_0)] is limited by availability of materials capable of handling harsh solar environment and mission requirements, such as controls, communications, navigation precision, and environmental predictability [22]. Previous multiobjective mission trade-off studies [22] and proposals [17–21] indicate that the perihelion approaches as close as $d_0 = 0.1$ AU (∼20 solar radii) from the sun are optimal for near-term missions to interstellar space. We note that determination of an optimal perihelion pass (0.1 AU or smaller) follows from a costly and laborious multiyear mission design process that takes many diverse factors into account, including among others science objectives, instrumentation, reliability, mission cost, solar environment, navigation, communications, and precision of spacecraft controls. We take the proposed [17–22] 0.1 AU perihelion as a guideline for a subsequent discussion of photonic materials design challenges (Sec. 3 and Sec. 5). However, we stress that the discussion below is applicable to even closer solar approaches (i.e., smaller perihelia).

3. MATERIAL AND DESIGN CHALLENGES

Flying as close as 0.1 AU (∼20 solar radii) from the sun [17–22] [Fig. 1(b)] a sail would experience more than 100 times the solar irradiance at Earth ($S_{1\,\mathrm{AU}} \simeq 1{,}360$ W/m^2). It is this high-power flux combined with a slingshot maneuver that enables high cruise velocities [17,18,22]. However, high sunlight flux also implies that even minute absorption might lead to excessive sail material heating. Furthermore, interaction with space plasma [45]—solar wind and other energetic particles—and high energy photons, can serve as an additional source of heat deposition [see Fig. 4(a)]. With radiative cooling being the sole mechanism for temperature regulation in space, it is of a critical importance to keep the balance between the heat generated due to optical absorption and interaction with space plasma on one hand (i.e., $P_{\mathrm{in}} = \alpha S + P$), and thermal radiation emission on the other (i.e., $P_{\mathrm{out}} = \sigma\epsilon T^4$). At equilibrium sail's temperature, T, at perihelion, d_0, may be found from a simple power balance as

$$T \simeq \left(\frac{\alpha}{\epsilon}\frac{S_{1\,\mathrm{AU}}}{\sigma}\frac{(1\,\mathrm{AU})^2}{d_0^2} + \frac{P}{\sigma}\right)^{\frac{1}{4}}, \quad (7)$$

where ϵ is the thermal emissivity of the sail material, σ is the Stefan-Boltzmann constant, and P is the heat flux deposited by solar wind and high energy particles emanating from the sun [see also Fig. 4(a)]; the emissivity is due to thermal radiation from the front and back sides of the sail: $\epsilon = \frac{1}{\sigma T^4}\int_0^\infty(\epsilon_{b,\lambda} + \epsilon_{f,\lambda})I_{BB}(T,\lambda)\mathrm{d}\lambda$, here for an ultrathin film sail a uniform temperature, T, across the sail is assumed, $\epsilon_{b,\lambda}$ and $\epsilon_{f,\lambda}$ are back and front side hemispherical spectral emissivities, respectively, $I_{BB}(T,\lambda) = (2hc^2/\lambda^5)(1/(\exp(hc/\lambda k_B T) - 1))$ is the spectral power density of the black body at a temperature T, h is the Plank constant, and k_B is the Boltzmann constant.

In a case when effects of solar plasma are negligible (i.e., $P \to 0$), thermal response is governed by the absorption of the incident solar flux, $P_{\mathrm{in}} \simeq \alpha S$, and thermal radiation emission into the free space, $P_{\mathrm{out}} = \sigma\epsilon T^4$. An optimal structure would therefore imply minimizing sunlight absorption, α, and maximizing sail thermal emissivity, ϵ, to keep sail temperature as low as possible. In addition to passive thermal regulation, sail materials should be reflective to ensure efficient transfer of photon momentum for radiation pressure propulsion [20]. Optimal pressure is achieved for $r \to 1$ and $\alpha \to 0$ [Eq. (5) and Sec. 2]. In this case, propulsive efficiency of the sail, $\eta = r + \frac{1}{2}\alpha$, is maximized. Minimizing sail temperature (i.e., by increasing sail emissivity) and maximizing its reflectivity set design constraints for sail materials.

Current solar sails are made of aluminized polymer films with ∼50−100 nm thick aluminum atop of a few micron thick polymer (e.g., CP1, Mylar, or Kapton) support layer [20,39–41] [Fig. 4(b)]. On average the aluminum facing side absorbs 8%–10% of sunlight reflecting the rest [46]. To illustrate the limitation of the current sail materials in Fig. 4(c) we plot the variation of the sail temperature at equilibrium with perihelion distance for two different solar absorptivities ($\alpha = 0.05$ and $\alpha = 0.15$) for thermal emissivity varying in a range from 0.1 to 1. A relatively low melting temperature of polymer substrates used in current solar sails limits the range of distances that a sail can reach (∼250 K for Mylar and CP1, and ≤670 K for Kapton, as indicated with dashed lines in Figs. 4(c) and 4(d) [47,48]. While Kapton-based sails owing to their higher melting point [47] can get closer to the sun, Kapton films are ≥5 μm thick, which makes them too heavy for advanced solar sail missions. For this purpose, thinner CP1 polymer films (2.5 μm thick) are presently used for solar sailing [39–41]. The emissivity of thin standalone polymer films used in present day solar sails is low. Thus, CP1 is nearly transparent across the infrared band [49] ($\epsilon = 0.45$ for a 1 mm thick film [48]), whereas emissivities of Kapton and Mylar films are $\epsilon < 0.25$ and $\epsilon < 0.15$, respectively, for 25 μm thick aluminum backed films [46]. Even lower values are anticipated for few micron thick films. Low emissivity of polymer films used in present day sails limits their use to missions with >0.4 AU perihelion (i.e., outside of Mercury orbit).

This is where engineering the solar sail backside emissivity may offer new opportunities for missions with smaller perihelia. Hence, by increasing backside thermal emissivity to $\epsilon_b > 0.8$ while retaining low overall aerial density, aluminized polymer sails may potentially enable missions with up to ∼0.2 AU perihelion, i.e., ∼40 solar radii. Such emissivity enhancement may be attained by carefully tuning infrared spectral properties of polymer materials [49–55], which are currently under development for a range of applications, including radiative cooling and thermal management. For example, [52] reports hierarchical polymer coatings with room temperature emissivity $\epsilon > 0.97$, whereas [49] demonstrates an ultrathin CP1 polymer-based film with an emissivity of $\epsilon = 0.65$ and an aerial density of 3.3 g/m^2. Use of carbon fillers

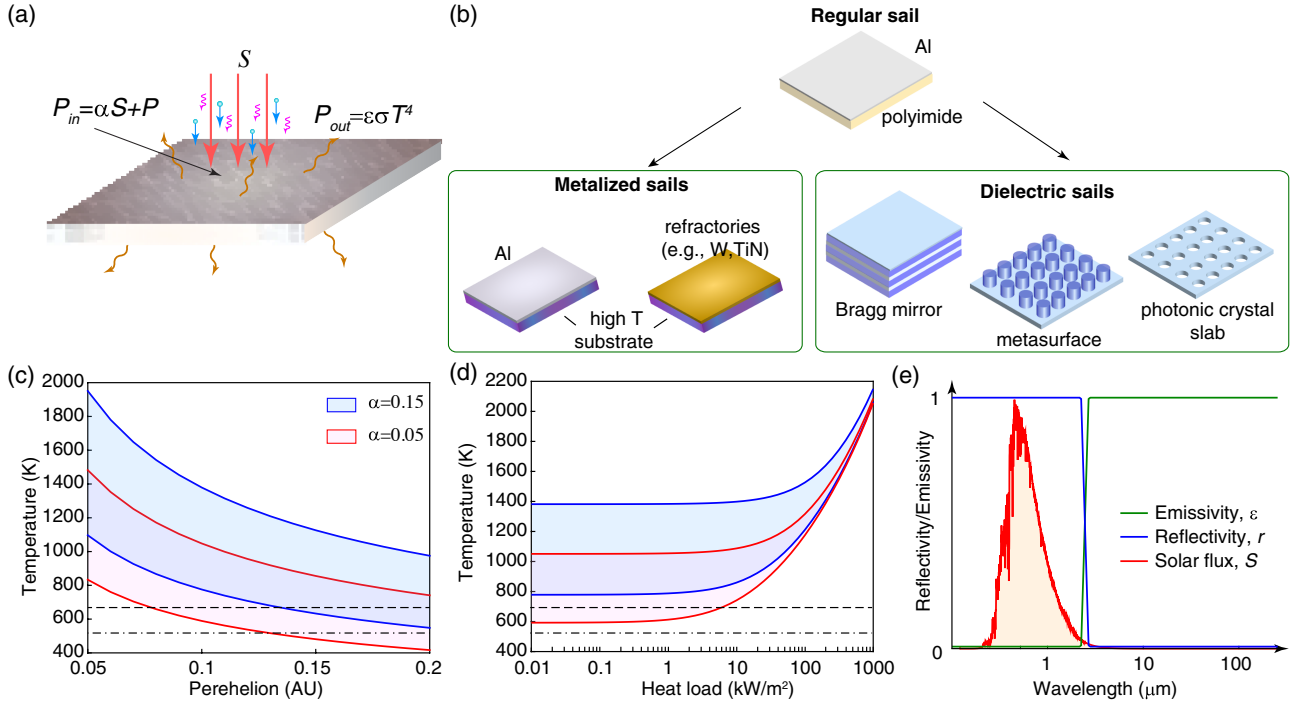

Fig. 4. Thermal management and sail design. (a) Power balance at equilibrium: sail interaction with incident solar flux, S, and other forms of radiation results in heat deposition ($P_{\rm in}=\alpha S+P$), while radiative cooling serves as the sole mechanism of heat damping ($P_{\rm out}=\sigma\epsilon T^4$). (b) An illustration of ideal reflectivity and emissivity (absorptivity) spectra. AM0 solar spectrum (i.e., $S_{1\,\rm AU}$) is also shown. (c) Sail temperature with perihelion distance for two values of solar absorptivity without account of solar plasma heat load, i.e., $P=0$. (d) Sail temperature variation at $d_0=0.1$ AU perihelion with heat load, P. In both panels (c) and (d) shaded areas correspond to a span of temperatures for a given solar absorptivity with emissivity varying from $\epsilon=0.1$ (upper bound) to $\epsilon=1$ (lower bound). Dashed lines denote the melting temperature of an aluminized polyimide sail—current technology. (e) Schematic illustration of a current sail design and potential nanophotonic structures, including Bragg mirrors, photonic crystal slabs, and metasurfaces.

in a polymer matrix is also examined for creating high emissivity films [54,55]. Further study of pathways to fabricating even lighter films (<1 g/m^2) with a near-unity infrared thermal emissivity that are suitable for high operating temperatures is needed. If such engineered polymer materials prove to be space qualified, these materials may become candidates for near-Sun solar sail missions.

For even closer approach to the sun (i.e., with perihelion $d_0\leq 0.2$ AU), where propulsion to higher excess velocities is expected [see Fig. 1(b)], novel high temperature sail materials are required. The need for high temperature materials was highlighted in several of previous works, where such options as graphene, beryllium, and dielectric sails were proposed [19,56,57]. We identify two conceptual approached to high temperature solar sail material design: metalized sails and dielectric sails [Fig. 4(b)]. Metalized sail designs resemble presently used aluminized polymer sails, where a front, sun-facing side is coated with a thin layer of metal that reflects most of the sunlight, whereas the backside serves as a high temperature support film, which also aids with thermal regulation via radiative cooling. For example, by substituting low temperature polymers with higher temperature (e.g., >1000 K) inorganic substrate materials, the operation temperature of aluminized sails increases to $\sim$900 K (limited by the melting point of Al itself). To obtain high backside emissivity, resonant infrared plasmonic structures and materials with strong phonon-polariton resonances in the midinfrared can be utilized [58–65]. For instance, many polar dielectrics, including SiC, SiO_2, and TiO_2, exhibit resonant absorption at 7–10 μm range [66]. A wide variety of designs have been discussed recently in the context of radiative cooling [58,63,65] and for spacecraft thermal management [49,61,62]. With a near-unity backside emissivity, $\epsilon_b\to 1$, such sails may get as close as 0.06 AU from the sun, thus satisfying objectives of near-term missions. Further studies would require design of nanophotonic structures stable at high operation temperatures ($\sim$1000 K and above) and design of ultralight and ultrathin films (i.e., <1 g/m^2).

Sail interaction with the solar wind and high energy particles [45] may result in a further increase of sail temperature [Fig. 4(d)] [67]. Such interaction may be described by an additional non-radiative heat deposited into a sail material, P. For thermal load $P\geq 1$ kW/m^2 sail interaction with space plasma has a noticeable effect on sail temperature. Additional consideration in thermal power balance and design of thermal emissivity is therefore needed. For a higher heat flux, $P\geq 100$ kW/m^2, which is comparable to a heat load observed in many of commonly used plasma systems [67,68], the temperature of a sail may exceed 1500 K, implying that only a limited number of refractory materials with high melting points should be used [69–78]. Only a handful of dielectrics and metals survive these extreme temperatures, further limiting a sail materials design space. Candidate optical materials suitable for these high operation temperatures include, among others, HfO_2, TiO_2, SiC, TiN, TiC, W, and Mo [71–78]. Photonic nanostructures made of TiN and W are actively studied for demanding nanophotonic applications, such as heat assisted magnetic recording [71] and thermophotovoltaics [76–78]. A standalone 100 nm-thick W film would reflect less than $\sim$60% and absorb more than 40% of sunlight [46], implying $\eta=80\%$ propulsion efficiency. However, as any metal, planar tungsten films possess relatively low thermal emissivity (tungsten has $\epsilon\simeq 0.03$ at

T = 300 K and $\epsilon \simeq 0.25$ at T = 2000 K [76], implying elevated operating temperatures (e.g., at 0.1 AU a standalone W film will have $T \geq 1400\ K$). Engineering thermal emissivity, for instance by structuring tungsten and other refractory metal films [76], or by back-coating with high-temperature thermally emissive layers [59], thus would be needed to decrease the operating temperature. Importantly, the high density of many refractory metals (e.g., for W mass density is 19.3 g/cm^3) contributes to the sail weight and challenges design of lightweight solar sails (i.e., leads to small A/m) that can be propelled to high velocities [Fig. 1(b)]. Lightweight refractory materials, e.g., TiN, might be more preferable [73] in this case. Noteworthy, that in practice, choice of sail materials would be governed by tradeoff studies for a given mission.

All-dielectric sails offer a conceptually different approach to highly reflective and low-loss sail materials [Fig. 4(b)]. Many optical dielectrics (e.g., SiO_2, $Al2O_3$, TiO_2, HfO_2, MgF_2) are high-temperature low-loss transparent materials, making them ideal for solar sails. By structuring and patterning dielectric materials at the dimensions comparable with the optical wavelength (∼200 nm) resonant photonic metamaterials with a desired optical dispersion (i.e., angular and spectral reflectances) may be created [79–81]. Planar all-dielectric Bragg mirrors offer a simple approach to reflectance engineering [Fig. 4(b)]. Mirrors with very broad band and very high reflectivity (>90%) with a wide acceptance angle (up to 30%) are commercially available [82,83]. However, such mirrors require multilayer stacking, more than 10 layers, resulting in relatively thick films (few microns) and, hence, higher sail aerial density and weight [84]. Patterned dielectric nanostructures, such as high contrast gratings [85], photonic crystal membranes [86,87], and all-dielectric metasurfaces [88–90] can be fabricated within a single layer of material providing a pathway to thinner (< 1 μm) and lighter reflectors [Fig. 4(b)]. Being resonant in nature [81], these structures, however, typically tend to exhibit narrower reflectance bands as compared to planar Bragg gratings and are sensitive to the angle of incidence. Hybrid designs that combine different types of nanostructures (e.g., Bragg stacks and metasurfaces) and materials (e.g., dielectrics and refractory metals) may offer a more optimal solar sail performance, i.e., larger A/m ratio and while maintaining broad band reflectivity. Inverse design of photonic structures and sophisticated optimization techniques might be needed for obtaining desired performance metrics [91–94].

At the same time, thermal regulation of ultrathin dielectric sails differs conceptually from the metalized ones. Whereas for metalized sails front and back sides are decoupled (as ∼100 nm thick metal films are nearly impermeable for visible and infrared radiation), in the case of dielectric sails the entire volume of material is interacting with the incident radiation. Therefore, the spectral response of dielectric sails should be chosen as a careful balance between solar absorptivity in one part of the spectrum (i.e., $\alpha_\lambda = \epsilon_\lambda \to 0$) and thermal emissivity in the other (i.e., $\epsilon_\lambda = \alpha_\lambda \to 1$). An idealized spectral response is described by step functions for r_λ and ϵ_λ (α_λ), as schematically shown in Fig. 4(e). In particular, $r = \frac{1}{S_{1\,\mathrm{AU}}} \int_0^{\lambda_c} S_{1\mathrm{AU},\lambda}(\lambda)\mathrm{d}\lambda$ and $\epsilon = \frac{2}{\sigma T^4} \int_{\lambda_c}^{\infty} I_{BB,\lambda}(T, \lambda)\mathrm{d}\lambda$, where crossover wavelength, λ_c, is found as a result of minimizing for sail temperature, T, and maximizing for its reflectivity, r (here factor 2 is due to $\epsilon_{b,\lambda} \simeq \epsilon_{f,\lambda}$ for ultrathin dielectric sails). This is where nanophotonic metamaterials [58,59] may offer a unique opportunity to independently engineer both visible and infrared spectral responses and optical dispersion (i.e., create thin film structures with sharp spectrally selective features that enable simultaneously high solar reflectivity and high thermal emissivity). In recent years, a number of structures with such spectrally selective properties have been shown in the context of radiative cooling [60,63–65]. With further design and optimization, such nanophotonic structures may enable solar sail missions with small perihelion approaches (<0.1 AU).

Mechanical strength of fabricated sail materials is another important design factor to consider. At 0.1 AU perihelion, one may expect at most 1 N load per every 1000 m^2 of sail material. By properly distributing the load with booms and spars, mechanical stresses across the sail materials may be further optimized. The minimum sail thickness can be estimated as $w = \frac{F}{\sigma_{\mathrm{UTS}}\, L}$, where F is the mechanical load, σ_{UTS} is the ultimate tensile strength of the sail material, and L is a characteristic dimension of a free-standing sail segment (e.g., sail length along the boom). For $F = 1$ N force acting on 1000 m^2 sail (i.e., $L \simeq 31.6$ m) with an ultimate tensile strength of $\sigma_{\mathrm{UTS}} = 10$ MPa (for comparison, the tensile strength of currently used CP1 polymer is 87 MPa [48]) we obtain $h \simeq 3.16$ nm, which suggests that ∼100 nm films can easily withstand anticipated loads during the perihelion pass. However, other considerations may emerge during film fabrication, sail packaging and assembly on Earth, and subsequent deployment in space. To ensure mechanical stability, delicate ultrathin films may be reinforced with the use of ultralight-weight microarchitectured scaffolds, such as nanocardboards [95] or cellular materials [96]. Notably, many materials that exhibit desired optical properties are naturally strong as well. For instance, TiN and SiO_2 have tensile strength >5 GPa [97,98], which suggests that large area thin free-standing films may be fabricated.

Finally, to attain sufficient acceleration of an instrument-laden sail, an area exceeding 10,000 m^2 may be needed [Fig. 1(b)]. The need for large area implies that designed photonic materials and structures should be compatible with very large-scale fabrication and/or assembly techniques. While large area thin film deposition is presently widely utilized for planar and layered materials growth [99], advances in scalable nanolithography, such as roll-to-roll nanoimprint lithography [100] would be needed to define desired photonic patterns over a large area. Self-assembly and solution processing may provide an alternative route [101]. However, these techniques would need to be optimized to enable high quality photonic structures with well-defined properties over large areas. Assembly and integration of smaller scale, e.g., wafer-sized structures, into a single film may be another possible solution. Laser and electron beam welding may be used for this purpose [102,103].

4. ACTIVE AND PASSIVE PHOTONIC CONTROL

In addition to a need for low-mass and high-reflectivity materials, taming the directionality and intensity of sunlight scattering is of great importance for controlling solar sail attitude, Fig. 5. At present, radiation pressure forces and associated sail dynamics are controlled by mechanical systems, such as $x-y$ translation tables that actively manage the center of mass versus the center of pressure [104]. These systems are rather bulky, adding to overall mass and complexity. Metamaterials [79–81] with their ability for agile control over light reflectance and transmittance provide a different approach [105–109]. Hence, by making use of passive and active structures that alter local optical properties, a desired distribution of radiation pressure may be attained to control overall

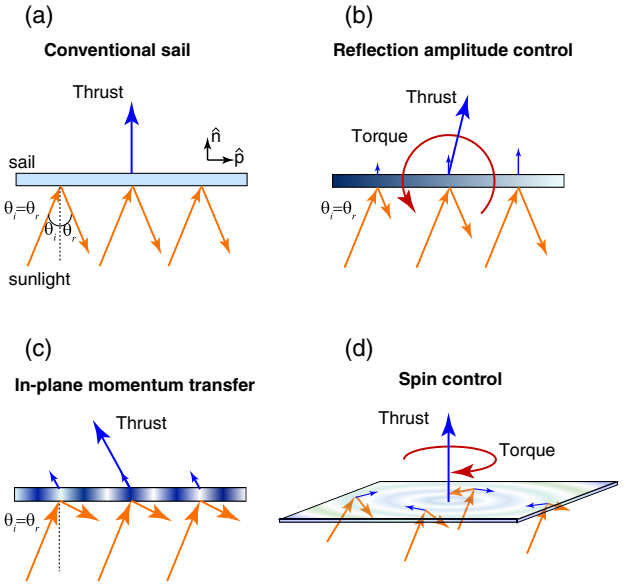

Fig. 5. Photonic designs for radiation pressure and momentum management. (a) Flat perfectly reflecting sails may impart thrust only in a direction normal to sail surface. For this reason, mechanical vanes that tilt to change the direction of thrust are used. (b) With the use of thin film surfaces with actively controlled intensity of local reflectance a desired distribution of radiation pressure may be attained to control thrust and torque. (c) Metasurfaces and diffraction gratings allow for light reflection at angles different from the incidence angle enabling thrust vector component in the plane of the sail. (d) Phase gradient surfaces may offer an additional pathway for momentum management by reflecting light out of the incidence plane. In this case, in-plane forces may be induced to control sail spin.

sail dynamics [Figs. 5(b)–5(d)]. Electrically tunable metasurfaces and devices are gaining interest due to their ability to manipulate optical phase and amplitude [110–114]. These semiconductor [110,111] and liquid crystal [112–114] devices are of a particular interest. Liquid crystal structures offer very high contrast switching of reflectance and are of a great promise for solar sail actuation due to their broadband and low power operation (<1 mW/cm^2) [114]. To maximize the effectiveness of such variable reflectance materials, they will likely be embedded within the sail along its outermost edge, requiring either localized power generation and wireless control, or the addition of long wire harnesses from the spacecraft bus that will increase complexity and mass.

For ultra-low power configurations, completely passive structures can be used for solar sail attitude control. As an example, diffraction gratings and metasurfaces can change the directionality of the incoming light [105–109]. As the direction of light propagation changes, so does the light's momentum. To counter-balance this change, the sail acquires the complementary momentum to ensure conservation, Figs. 5(c) and 5(d). Thus, having arbitrary control of the reflection or refraction can enable efficient momentum transfer and arbitrary control of the sail, allowing for not only forward propulsion, but also the ability to raise and lower the sail's orbit [109].

In particular, for planar diffraction grating sails [107–109], the thrust vector will be directed along $\boldsymbol{\eta} = \cos\theta_i(\cos\theta_i + \cos\theta_n)\hat{\boldsymbol{n}} + (n\lambda/\Lambda)\hat{\boldsymbol{p}}$, where θ_i is the angle at which sunlight subtends the normal vector of the sail, $\hat{\boldsymbol{n}}$, θ_n is the diffraction angle, λ is the light wavelength, Λ is the grating period, n is the diffraction order, and $\hat{\boldsymbol{p}}$ is a unit vector perpendicular to $\hat{\boldsymbol{n}}$. Because $\hat{\boldsymbol{p}}$ is in the plane of the sail, a new perpendicular thrust vector emerges, which provides an additional control mechanism. To make the most efficient use of the sun, it is preferable to have the sail facing the sun, i.e., with $\theta_i = 0$. For interstellar missions, both a reflecting sail and a zero-order diffracting sail provide an efficient momentum transfer along the sunline. For interplanetary or solar polar orbiting [6–10] missions, the use of diffraction gratings with $\theta_n = 90°$ is preferable. In this case, a large force may be achieved perpendicular to the sunline, as required for a spiral trajectory, Fig. 5(c). Recently free-standing ultrathin (potentially as thin as 200 nm) liquid crystal polymer-based diffraction gratings with a broadband and near unity efficiency have been developed. Such structures may be of interest for passive and active diffractive solar sails [115,116].

With an ability to control light reflectance out of its incidence plane, metasurfaces [80] enable imparting radiation pressure forces in any direction within the sail plane, providing a very promising mechanism for controlling sail spin and its orientation, Fig. 5(d). This approach is conceptually different from translating mass systems [104] developed for near-term missions [39–41] and shows great promise for use in future crafts.

5. EFFECTS OF SPACE ENVIRONMENT

Powered slingshot maneuver needed to accelerate a sail to very high velocity, implies that a sail would fly in close proximity to the sun: ~ 0.1 AU or about 20 solar radii from sun's surface. Although outside the reach of the solar corona [14,45], a sail spacecraft would interact with the solar wind, the density and temperature of which grows in the vicinity of the sun. Specifically, at 0.1 AU it is expected [117] that ions (mostly H with $\sim$5% of He) would have velocities $\sim 100 - 1000$ km/s, which depend on the solar longitude [45]. Solar plasma would also have electron temperature of $T_e \simeq 10^6$ K and plasma density of 10^3 cm^{-3}, i.e., >300 times larger than at Earth orbit. The low energy of the solar plasma (0.5–10 keV) implies a shallow depth of ion penetration, only several to tens of atomic layers, causing sputtering of surface layers, radiation enhanced sublimation, and potentially ablation [67,68]. Insolubility of He and H ions in the materials would cause formation of nanoscale bubbles leading to structural deformation and materials exfoliation [118,119]. Another important metric to consider is the rate of energy deposition by plasma and high energy photons (e.g., in Hall thrusters ion implantation within electrode materials may cause more than 100 kW/m^2 of heat generation [67,118]). While low energy deposition rates predominantly lead to materials heating, higher rates might cause plastic deformation, bulk and surface diffusion, and potentially melting and evaporation of sail materials [118]. Figure 6 highlights some of the possible effects of sail material degradation when subject to a solar radiation environment. Development of solar sails resistant to solar plasma, high heat loads, and high energy radiation may be informed by a large body of expertise in the design of materials for highly corrosive environments, such as high-power ion and Hall thrusters [67], fusion reactor walls, coatings of hypersonic vehicles [118], and more recently Solar Parker Probe heat shield [14]. Refractory and rare-Earth metals (e.g., W, Mo, Re, Ta), refractory ceramic materials (e.g., HfC, SiC, TaC, ZrO_2, ZrN), and carbon are particularly suited for these applications [67,69,70,118,119], a number of studies have shown that by micro- and nanostructuring of material surfaces effects of radiation damage may be reduced by 30%–50% [118,119]. Microarchitectured surfaces distribute heat and ion implantation more evenly throughout the material, reduce the

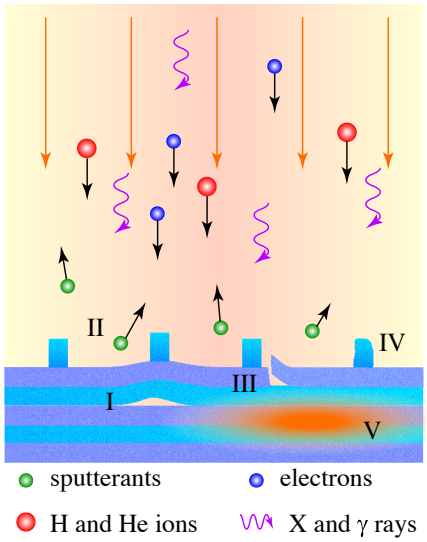

Fig. 6. Effects of solar plasma and energetic photons and particles on nanophotonic structures: (I) formation of bubbles, (II) surface sputtering, (III) cracking, exfoliation and delamination, (IV) surface morphology deformation, and (V) energy deposition and thermos-mechanical stresses.

implanted ion atom residence time, and reduce thermal stresses, as compared to planar smooth surfaces [106]. However, the need for ultrathin ($\leq$1 μm) and low aerial density ($\leq$1 g/m^2) solar sail materials [20] that exhibit low sunlight absorbance (desirably $\ll$10%) pose additional constrains. Indeed, plasma interaction with nanophotonic structures, particularly, thin film heterostructures, its influence on structural stability and optical performance is yet to be understood. Further research effort in this direction is needed.

6. OTHER CONSIDERATIONS

While an overview of solar sail photonic material challenges is the main focus of this perspective, successful interstellar missions require development of other spacecraft systems, including efficient sail deployment mechanisms, power systems, deep space communications, and precise navigation. Each of the aforementioned areas is a complex field on its own with a number of engineering and foundational challenges. Their detailed discussion is beyond the scope of this review. Here, we provide a brief insight into some of the key issues.

Propulsion of a 10–50 kg payload carrying scientific instruments, power and communication systems to >20 AU/year would require large area sails, $A > 10{,}000$ m^2. Development of such large area sails is under way (see Fig. 2). For example, Solar Cruiser—a recently approved heliophysics mission scheduled for 2025—will feature sail area with $A > 1600$ m^2 (A/m < 20 m^2/kg) [40,41]. However, design of even larger sails with a higher sail area to mass ratio faces challenges associated with sail stowage, deployment, and testing [120,121]. Further study of lightweight support booms and mechanically compliant mechanisms [122] informed by novel manufacturing techniques [123], and advances in composite materials is needed [124,125].

Moving beyond Jupiter orbit challenges harvesting of solar radiation for powering of spacecraft systems [22,25,27,126]. This is where a renewed effort on redesigning radioisotope thermoelectric generators for smaller mass and higher efficiency is particularly important. Emergent thermoelectric materials and nanostructures [127,128] may find use in such systems.

Communications and navigation present yet another challenge for spacecraft operation beyond 100 AU [22,25,129]. Optical communication links for deep space exploration are being examined and tested [130]. Several technology demonstration missions, including a Psyche mission planned for 2022, will test deep space optical communication [131]. Future systems may benefit from light-weight optical systems, such as metasurfaces [79–81], high efficiency integrated optics laser sources, and tunable optical oscillators with an ultranarrow linewidth [132].

7. LASER SAILING

Laser sailing [133–139], including a most recent proposal [25], is another approach extensively examined for interstellar flight. Although laser sails, similarly to solar sails, make use of radiation pressure for propulsion, their requirements on sail materials, systems engineering, and concept of operations are *drastically different* from those of solar sails [25–27]. A recent review [26] highlights key photonic challenges facing development of laser sail materials. Specifically, laser sails need to handle much higher power levels (e.g., ~100 GW/m^2 as in [25] in the near infrared wavelength range ($\lambda \in [1\ \mu m,\ 1.5\ \mu m]$) defined by the atmospheric transparency window and Doppler shifting. This leads to very different material requirements for laser sail design. For instance, in contrast to solar sails, high refractive index semiconductors such as Si and MoS_2 may be used for the laser sailing. Such materials are highly absorbing across the solar spectrum and thus cannot be utilized for solar sailing.

In addition, limited range of laser beaming, constrained by beam diffraction and laser aperture size [25,27], poses limitations on the acceleration distance, which, in turn, constrains the laser sail design [26]. For example, to circumvent these limitations an ultralight-weight (~1 g) laser sail spacecraft was proposed in [25], which puts very stringent requirements on sail shape, optical properties, and mass density [26]. Solar sails are free of these constrains and offer an optimal performance when it comes for mass per velocity as compared to both laser sails [25–27,133–139] and other near-term propulsion methods [28–32]. In particular, in comparison to laser sails, solar sails can carry orders of magnitude heavier payload (up to ~100 kg), while offering higher cruise velocity as compared to other propulsion methods (≥5 times faster).

8. CONCLUSIONS AND OUTLOOK

We have discussed the promise of solar sailing for fast, accessible, and scalable space exploration beyond the limits of current propulsion technologies. Without the need to carry on board propellant, solar sails offer an efficient pathway for space travel. Solar polar orbiters and interstellar probes are some of the potential missions, where solar sails promise an unmatched potential compared to conventional chemical and electric means of propulsion. Our analysis shows that with a research and development effort solar sails that can reach <0.1 AU may be built. In Fig. 7 we sketch a photonic materials research and development roadmap, highlighting the areas where a focused effort is needed to enable next generation solar sails for future interstellar missions. Future progress in solar sailing would require the development of novel active and passive materials to meet demanding requirements of the space environment, sail control, and navigation. We showed

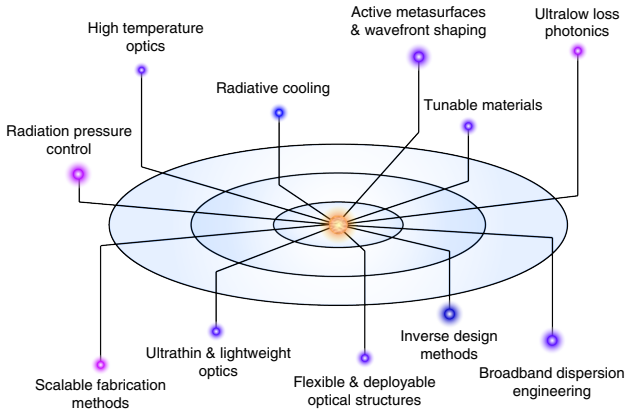

Fig. 7. Interstellar solar sail materials roadmap. The roadmap is inspired by a map of neighborhood stars. The distance indicates the technology readiness: the farther away from the center (i.e., present) the more research effort is needed.

that thin film photonic metamaterials and diffraction gratings may pave the way to novel multifunctional materials with enhanced capabilities for thermal management, reflectivity, and momentum control. Future high temperature photonic materials may enable close solar flyby for missions examining solar atmosphere and for boosting towards interstellar space with unprecedented speed. Metamaterials that can efficiently control the reflection and transmission properties may provide novel solutions for solar sail dynamics and attitude control. In this perspective, we have focused on key areas where further research in materials science and nanophotonics is necessary to push the limits of solar sail technology. In addition to photonic materials, future solar sails would benefit from more efficient architecture design and integration with lightweight support structures and deployment mechanisms [115]. Inherently limited mass budget will also stimulate research and development of lightweight and multifunctional payload components, including instruments, communication, and navigation systems.

We envision that with further advances in optical materials science and nanotechnology the next generation of solar sails may pave the way for breakthrough space exploration missions.

Funding. National Aeronautics and Space Administration (80NSSC19K0975, 80NSSC20K1021, NNX12AQ50G, NNX15AW53A).

Acknowledgment. The authors thank the NASA Innovative Advanced Concepts (NIAC) program and the Optical Society of America (OSA) Incubator meetings. G.A.S. is also thankful to the Gordon and Betty Moore Foundation, the National Science Foundation, the Air Force Office of Scientific Research, Sydor Optics, and ThorLabs. A.R.D. also acknowledges useful discussions with L. Friedman.

Disclosures. The authors declare no conflicts of interest.

Data Availability. Data underlying the results presented in this paper are not publicly available at this time but may be obtained from the authors upon reasonable request.

REFERENCES

1. R. Forward, "Starwisp—an ultra-light interstellar probe," J. Spacecr. **22**, 345 (1985).
2. P. C. Liewer, R. A. Mewaldt, J. A. Ayon, and R. A. Wallace, "NASA's interstellar probe mission," in *CP504 Space Technology and Applications International Forum-2000* (2000).
3. K. Long, "Interstellar probes: the benefits to astronomy and astrophysics," arXiv:1901.04422 (2019).
4. R. L. McNutt, R. F. Wimmer-Schweingruber, M. Gruntman, S. M. Krimigis, E. C. Roelof, P. C. Brandt, S. R. Vernon, M. V. Paul, B. W. Lathrop, D. S. Mehoke, D. H. Napolillo, and R. W. Stoughl, "Near-term interstellar probe: first step," Acta Astronaut. **162**, 284 (2019).
5. R. J. Litchford and J. A. Sheehy, "Prospects for interstellar travel," in *43rd Annual AAS Guidance, Navigation and Control Conference*, Breckenridge, Colorado, USA (2020), pp. AAS 20-068.
6. B. E. Goldstein, A. Buffington, A. C. Cummings, R. Fisher, B. V. Jackson, P. C. Liewer, R. A. Mewaldt, and M. Neugebauer, "A solar polar sail mission: report of a study to put a scientific spacecraft in a circular polar orbit about the sun," Proc. SPIE **3442**, 65–76 (1998).
7. G. Colangelo, O. Pace, R. Marsden, and B. Fleck, "Solar orbiter: a challenging mission design for near-sun observations," ESA Bull. **104**, 76–85 (2000).
8. B. Dachwald, A. Ohndorf, and B. Wie, "Solar sail trajectory optimization for the solar polar imager (SPI) mission," in *AIAA/AAS Astrodynamics Specialist Conference and Exhibit*, Keystone, Colorado, USA, August, 2006, pp. AIAA 2006-6177.
9. M. Macdonald, G. W. Hughes, C. R. McInnes, A. Lyngvi, P. Falkner, and A. Atzei, "Solar polar orbiter: a solar sail technology reference study," J. Spacecr. Rockets **43**, 960 (2006).
10. A. Dubill, "Attitude control for circumnavigating the sun with diffractive solar sails," thesis (Rochester Institute of Technology, 2020).
11. A. A. Siddiqi, "Deep space chronicle: a chronology of deep space and planetary probes 1958–2000, monograph in aerospace history," NASA SP-2002-4524 (2002), p. 24.
12. E. Stone, "The voyagers," Nat. Astron. **1**, 896 (2017).
13. R. Du Toit Strauss, "Voyager 2 enters interstellar space," Nat. Astron. **3**, 963–964 (2019).
14. "Parker solar probe," NASA NP-2018-06-224-GSFC (2018).
15. J. L. Wright and J. Warmke, "Solar sail mission applications," in *AIAA/ASS Astrodynamics Conference*, San Diego, California, USA, August 18–20, 1976.
16. G. L. Matloff and E. F. Mallove, "The interstellar solar sail: optimization and further analysis," J. Br. Interplanetary Soc. **36**, 201–209 (1983).
17. C. Sauer, "Solar sail trajectories for solar-polar and interstellar probe missions," in *AAS/AIAA Astrodynamics Specialist Conference*, Girdwood, Alaska, USA (1999), pp. 99–1367.
18. B. Dachwald, "Optimal solar sail trajectories for missions to the outer solar system," J. Guidance, Control Dyn. **28**, 1187 (2005).
19. G. L. Matloff, "Graphene: the ultimate interstellar solar sail material?" J. Br. Interplanetary Soc. **65**, 378 (2012).
20. G. Vulpetti, L. Johnson, and G. L. Matloff, *Solar Sails. A Novel Approach to Interplanetary Travel* (Springer, 2015).
21. G. Swartzlander, L. Johnson, and B. Betts, "Light sailing into the great beyond," Opt. Photon. News **31**, 30–37 (2020).
22. S. G. Turyshev, M. Shao, V. T. Toth, L. D. Friedman, L. Alkalai, D. Mawet, J. Shen, M. R. Swain, H. Zhou, H. Helvajian, T. Heinsheimer, S. Janson, Z. Leszczynski, J. McVey, D. Garber, A. Davoyan, S. Redfield, and J. R. Males, "Direct multipixel imaging and spectroscopy of an exoplanet with a solar gravity lens mission," arXiv:2002.11871 (2020).
23. L. Johnson, R. M. Young, and E. E. Montgomery, IV, "Status of solar sail propulsion: moving toward an interstellar probe," MFC-426-Paper (2006).
24. D. Ma, J. Murray, and J. N. Munday, "Controllable propulsion by light: steering a solar sail via tunable radiation pressure," Adv. Opt. Mater. **5**, 1600668 (2017).
25. P. Lubin, "A roadmap to interstellar flight," J. Br. Interplanetary Soc. **69**, 40 (2016).
26. H. A. Atwater, A. R. Davoyan, O. Ilic, D. Jariwala, M. C. Sherrott, C. M. Went, W. S. Whitney, and J. Wong, "Materials challenges for the starshot lightsail," Nat. Mater. **17**, 861 (2018).
27. K. L. Parkin, "The breakthrough starshot system model," Acta Astronautica **152**, 370 (2018).
28. R. W. Lyman, M. E. Ewing, R. S. Krishnan, D. M. Lester, and R. L. McNutt, "Solar thermal propulsion for an interstellar probe," AIAA 2001-3377 (2001).
29. L. Alkalai, N. Arora, S. Turyshev, M. Shao, S. Weinstein-Weiss, M. Opher, and S. Redfield, "A vision for planetary and exoplanets science: exploration of the interstellar medium —the space between stars," in *68th International Astronautical Congress*, Adelaide, Australia (2017).
30. K. A. Von Ehricke, "Saturn-Jupiter rebound—a method of high-speed spacecraft ejection from the solar system," J. Br. Interplanetary Soc. **25**, 561–571 (1972).

31. G. Matloff and K. Parks, "Interstellar gravity assist propulsion: a correction and a new application," J. Br. Interplanetary Soc. **41**, 519–526 (1988).
32. K. Nock, "TAU—a mission to a thousand astronomical units," in *Presented at 19th AIAA/DGLR/JSASS International Electric Propulsion Conference*, Colorado Springs, Colorado, USA, May 11–13, 1987, paper AIAA-87-1049.
33. A. Witze, "Pluto fly-by: a graphical guide to the historic mission," Nature **523**, 140–141 (2015).
34. E. Witten, "Searching for a black hole in the outer solar system," arXiv:2004.14192 (2020).
35. O. Mori, Y. Shirasawa, Y. Mimasu, Y. Tsuda, H. Sawada, T. Saiki, T. Yamamoto, K. Yonekura, H. Hoshino, J. Kawaguchi, and R. Funase, "Overview of IKAROS mission," in *Advances in Solar Sailing* (Springer 2014), pp. 25–43.
36. https://www.dupont.com/content/dam/dupont/amer/us/en/products/ei-transformation/documents/DEC-Kapton-HN-datasheet.pdf.
37. J. Mansell, D. A. Spencer, B. Plante, A. Diaz, M. Fernandez, J. Bellardo, B. Betts, and B. Nye, "Orbit and attitude performance of the lightsail 2 solar sail spacecraft," in *AIAA Scitech 2020 Forum*, Orlando, Florida, USA, January 6–10, 2020, paper AIAA 2020-2177.
38. http://www.lookpolymers.com/pdf/NeXolve-LaRC-CP1-Polyimide.pdf.
39. L. McNutt, L. Johnson, D. Clardy, J. Castillo-Rogez, A. Frick, and L. Jones, "Near-earth asteroid scout," in *AIAA SPACE 2014 Conference and Exposition*, San Diego, California, USA (2014), paper AIAA 2014-4435.
40. C. L. Johnson, A. F. Heaton, F. M. Curran, and R. Dissly, "The solar cruiser mission: demonstrating large solar sails for deep space missions," in *Presentation at the 70th International Astronautical Congress*, Washington D.C., USA, October 21–25, 2019.
41. K. Kobayashi, L. Johnson, H. D. Thomas, S. McIntosh, D. McKenzie, J. Newmark, A. Heaton, J. Carr, M. Baysinger, Q. Bean, L. Fabisinski, P. Capizzo, K. Clements, S. Sutherlin, J. Garcia, K. Medina, and D. Turse, "The high inclination solar mission," arXiv:2006.03111v1 (2020).
42. D. A. Vallado, *Fundamentals of Astrodynamics and Applications*, 4th ed. (Microcosm, 2013).
43. H. Curtis, *Orbital Mechanics for Engineering Students*, 4th ed. (Butterworth-Heinemann, 2019).
44. J. R. Brophy, M. D. Rayman, and B. Pavri, "Dawn: an ion-propelled journey to the beginning of the solar system," in *IEEE Aerospace Conference* (2008), pp. 1–10.
45. M.-B. Kallenrode, *Space Physics: An Introduction to Plasmas and Particles in the Heliosphere and Magnetospheres*, Advanced texts in physics (Springer, 2004).
46. J. H. Henninger, "Solar absorptance and thermal emittance of some common spacecraft thermal control coatings," NASA Reference Publication 1121 (1984).
47. "KaptonTM manufacturer specifications," https://www.dupont.com/content/dam/dupont/amer/us/en/products/ei-transformation/documents/EI-10173-Kapton-EN-Data-Sheet.pdf.
48. "CP1TM manufacturer specifications," http://www.nexolvematerials.com/low-cure-polyimides/cp1-polyimide.
49. A. Naqavi, S. P. Loke, M. D. Kelzenberg, D. M. Callahan, T. Tiwald, E. C. Warmann, P. Espinet-González, N. Vaidya, T. A. Roy, J.-S. Huang, T. G. Vinogradova, and H. A. Atwater, "Extremely broadband ultralight thermally-emissive optical coatings," Opt. Express **26**, 18545–18562 (2018).
50. T. Okada, R. Ishige, and S. Ando, "Analysis of thermal radiation properties of polyimide and polymeric materials based on ATR-IR spectroscopy," J. Photopolym. Sci. Technol. **29**, 251–254 (2016).
51. Y. Zhai, Y. Ma, S. N. David, D. Zhao, R. Lou, G. Tan, R. Yang, and X. Yin, "Scalable-manufactured randomized glass-polymer hybrid metamaterial for daytime radiative cooling," Science **355**, 1062–1066 (2017).
52. J. Mandal, Y. Fu, A. C. Overvig, M. Jia, K. Sun, N. N. Shi, H. Zhou, X. Xiao, N. Yu, and Y. Yang, "Hierarchically porous polymer coatings for highly efficient passive daytime radiative cooling," Science **362**, 315–319 (2018).
53. L. M. Lozano, S. Hong, Y. Huang, H. Zandavi, Y. A. El Aoud, Y. Tsurimaki, J. Zhou, Y. Xu, R. M. Osgood, G. Chen, and S. V. Boriskina, "Optical engineering of polymer materials and composites for simultaneous color and thermal management," Opt. Mater. Express **9**, 1990–2005 (2019).
54. Y. Sun, H. Chang, J. Hu, Y. Wang, Y. Weng, C. Zhang, S. Niu, L. Cao, Z. Chen, N. Guo, J. Liu, J. Chi, G. Li, and L. Xiao, "Large-scale multifunctional carbon nanotube thin film as effective mid-infrared radiation modulator with long-term stability," Adv. Opt. Mater. **9**, 2001216 (2021).
55. C. Larciprete, S. Paoloni, N. Orazi, F. Mercuri, M. Orth, Y. Gloy, M. Centini, R. Li Voti, and C. Sibilia, "Infrared emissivity characterization of carbon nanotubes dispersed poly(ethylene terephthalate) fibers," Int. J. Thermal Sci. **146**, 106109 (2019).
56. G. A. Landis, "Advanced solar-and laser-pushed lightsail concepts," in *NIAC* (1999).
57. R. Y. Kezerashvili and G. L. Matloff, "Solar radiation and the beryllium hollow-body sail: 1. The ionization and disintegration effect," J. Br. Interplanetary Soc. **60**, 169–179 (2007).
58. W. Li and S. Fan, "Nanophotonic control of thermal radiation for energy applications [Invited]," Opt. Express **26**, 15995–16021 (2018).
59. D. G. Baranov, Y. Xiao, I. A. Nechepurenko, A. Krasnok, A. Alù, and M. A. Kats, "Nanophotonic engineering of far-field thermal emitters," Nat. Mater. **18**, 920–930 (2019).
60. A. Howes, J. R. Nolen, J. D. Caldwell, and J. Valentine, "Near-unity and narrowband thermal emissivity in balanced dielectric metasurfaces," Adv. Opt. Mater. **8**, 1901470 (2020).
61. K. Sun, C. A. Riedel, Y. Wang, A. Urbani, M. Simeoni, S. Mengali, M. Zalkovskij, B. Bilenberg, C. H. de Groot, and O. L. Muskens, "Metasurface optical solar reflectors using AZO transparent conducting oxides for radiative cooling of spacecraft," ACS Photon. **5**, 495–501 (2018).
62. K. Sun, C. A. Riedel, A. Urbani, M. Simeoni, S. Mengali, M. Zalkovskij, B. Bilenberg, C. H. de Groot, and O. L. Muskens, "VO_2 thermochromic metamaterial-based smart optical solar reflector," ACS Photon. **5**, 2280–2286 (2018).
63. A. P. Raman, M. A. Anoma, L. Zhu, E. Rephaeli, and S. Fan, "Passive radiative cooling below ambient air temperature under direct sunlight," Nature **515**, 540–544 (2014).
64. L. Zhu, A. Raman, and S. Fan, "Color-preserving daytime radiative cooling," Appl. Phys. Lett. **103**, 223902 (2013).
65. J.-L. Kou, Z. Jurado, Z. Chen, S. Fan, and A. J. Minnich, "Daytime radiative cooling using near-black infrared emitters," ACS Photon. **4**, 626−630 (2017).
66. D.-Z. A. Chena and G. Chen, "Measurement of silicon dioxide surface phonon-polariton propagation length by attenuated total reflection," Appl. Phys. Lett. **91**, 121906 (2007).
67. A. Ottaviano, G. Z. Li, C. E. Huerta, A. Thuppul, Z. Chen, C. A. Dodson, and R. E. Wirz, "Plasma-material interactions for electric propulsion: challenges, approaches and future," in *The 36th International Electric Propulsion Conference*, Austria, September 15–20, 2019, paper IEPC-2019-517.
68. A. J. Lichtenberg and M. A. Lieberman, *Principles of Plasma Discharges and Materials Processing*, 2nd ed. (Wiley, 2005).
69. G. W. Meetham and M. H. Van de Voorde, *Materials for High Temperature Engineering Applications* (Springer, 2001).
70. J. Binner, M. Porter, B. Baker, J. Zou, V. Venkatachalam, V. R. Diaz, A. D'Angio, P. Ramanujam, T. Zhang, and T. S. R. C. Murthy, "Selection, processing, properties and applications of ultra-high temperature ceramic matrix composites, UHTCMCs–a review," in *International Materials Review* (2019).
71. U. Guler, A. Boltasseva, and V. M. Shalaev, "Refractory plasmonics," Science **344**, 263–264 (2014).
72. A. Banerjee, R. M. Heath, D. Morozov, D. Hemakumara, U. Nasti, I. Thayne, and R. H. Hadfield, "Optical properties of refractory metal based thin films," Opt. Mater. Express **8**, 2072–2088 (2018).
73. W. Li, U. Guler, N. Kinsey, G. V. Naik, A. Boltasseva, J. Guan, V. M. Shalaev, and A. V. Kildishev, "Refractory plasmonics with titanium nitride: broadband metamaterial absorber," Adv. Mater. **26**, 7959–7965 (2014).
74. K. Chaudhuri, M. Alhabeb, Z. Wang, V. M. Shalaev, Y. Gogotsi, and A. Boltasseva, "Highly broadband absorber using plasmonic titanium carbide (MXene)," ACS Photon. **5**, 1115–1122 (2018).
75. M. Minissale, C. Pardanaud, R. Bisson, and L. Gallais, "The temperature dependence of optical properties of tungsten in the visible and near-infrared domains: an experimental and theoretical study," J. Phys. D **50**, 455601 (2017).

76. I. Celanovic, N. Jovanovic, and J. Kassakian, "Two-dimensional tungsten photonic crystals as selective thermal emitters," Appl. Phys. Lett. **92**, 193101 (2008).
77. Z. Omair, G. Scranton, L. M. Pazos-Outón, T. P. Xiao, M. A. Steiner, V. Ganapati, P. F. Peterson, J. Holzrichter, H. Atwater, and E. Yablonovitch, "Ultraefficient thermophotovoltaic power conversion by band-edge spectral filtering," Proc. Natl. Acad. Sci. USA **116**, 15356–15361 (2019).
78. R. Sakakibara, V. Stelmakh, W. R. Chan, M. Ghebrebrhan, J. D. Joannopoulos, M. Soljacic, and I. Čelanović, "Practical emitters for thermophotovoltaics: a review," J. Photon. Energy **9**, 1 (2019).
79. S. Jahani and J. Zubin, "All-dielectric metamaterials," Nat. Nanotechnol. **11**, 23–36 (2016).
80. S. M. Kamali, E. Arbabi, A. Arbabi, and A. Faraon, "A review of dielectric optical metasurfaces for wavefront control," Nanophotonics **7**, 1041–1068 (2018).
81. A. I. Kuznetsov, A. E. Miroshnichenko, M. L. Brongersma, Y. S. Kivshar, and B. Luk'yanchuk, "Optically resonant dielectric nanostructures," Science **354**, aag2472 (2016).
82. J. W. Leem, X.-Y. Guan, and J. S. Yu, "Tunable distributed Bragg reflectors with wide-angle and broadband high-reflectivity using nanoporous/dense titanium dioxide film stacks for visible wavelength applications," Opt. Express **22**, 18519–18526 (2014).
83. W. Pacuski, C. Kruse, S. Figge, and D. Hommel, "High-reflectivity broadband distributed Bragg reflector lattice matched to ZnTe," Appl. Phys. Lett. **94**, 191108 (2009).
84. Y. Shen, D. Ye, I. Celanovic, S. G. Johnson, J. D. Joannopoulos, and M. Soljačić, "Optical broadband angular selectivity," Science **343**, 1499–1501 (2014).
85. C. J. Chang-Hasnain and W. Yang, "High-contrast gratings for integrated optoelectronics," Adv. Opt. Photon. **4**, 379–440 (2012).
86. V. Lousse, W. Suh, O. Kilic, S. Kim, O. Solgaard, and S. Fan, "Angular and polarization properties of a photonic crystal slab mirror," Opt. Express **12**, 1575–1582 (2004).
87. J. P. Moura, R. A. Norte, J. Guo, C. Schäfermeier, and S. Gröblacher, "Centimeter-scale suspended photonic crystal mirrors," Opt. Express **26**, 1895–1909 (2018).
88. P. Moitra, B. A. Slovick, W. Li, I. I. Kravchencko, D. P. Briggs, S. Krishnamurthy, and J. Valentine, "Large-scale all-dielectric metamaterial perfect reflectors," ACS Photon. **2**, 692–698 (2015).
89. H. Yang, H. Liu, B. Song, Y. Li, D. Meng, B. Chen, P. Hu, Y. Wang, T.-H. Ou, M. L. Povinelli, and W. Wu, "Effects of roughness and resonant-mode engineering in all-dielectric metasurfaces," Nanophotonics (to be published).
90. H. Atikian, P. Latawiec, X. Xiong, S. Meesala, S. Gauthier, D. Wintz, J. Randi, D. Bernot, S. DeFrances, J. Thomas, M. Roman, S. Durrant, F. Capasso, and M. Loncar, "Diamond mirror for high power lasers," arXiv:1909.06458 (2019).
91. S. Molesky, Z. Lin, A. Y. Piggott, W. Jin, J. Vucković, and A. W. Rodriguez, "Inverse design in nanophotonics," Nat. Photonics **12**, 659–670 (2018).
92. S. Jafar-Zanjani, S. Inampudi, and H. Mosallaei, "Adaptive genetic algorithm for optical metasurfaces design," Sci. Rep. **8**, 11040 (2018).
93. T. Phan, D. Sell, E. W. Wang, S. Doshay, K. Edee, J. Yang, and J. A. Fan, "High-efficiency, large-area, topology-optimized metasurfaces," Light Sci. Appl. **8**, 48 (2019).
94. W. Jin, W. Li, M. Orenstein, and S. Fan, "Inverse design of lightweight broadband reflector for efficient lightsail propulsion," ACS Photon. **7**, 2350–2355 (2020).
95. C. Lin, S. M. Nicaise, D. E. Lilley, J. Cortes, P. Jiao, J. Singh, M. Azadi, G. G. Lopez, M. Metzler, P. K. Purohit, and I. Bargatin, "Nanocardboard as a nanoscale analog of hollow sandwich plates," Nat. Commun. **9**, 4442 (2018).
96. T. A. Schaedler and W. B. Carter, "Architected cellular materials," Annu. Rev. Mater. Res. **46**, 187–210 (2016).
97. T. Hashishin, T. Kanawa, Y. Kaneko, and H. Iwanaga, "Morphology and tensile strength of titanium nitride whiskers," J. Ceram. Soc. Jpn. **105**, 1042–1046 (1997).
98. G. S. Glesemann, "Optical fiber mechanical reliability. Review of research at Corning's optical fiber strength laboratory, white paper," WP8002 (2017).
99. J. Greener, G. Pearson, and M. Cakmak, *Roll-to-Roll Manufacturing: Process Elements and Recent Advances* (Wiley 2018).
100. N. Kooy, K. Mohamed, L. T. Pin, and O. S. Guan, "A review of roll-to-roll nanoimprint lithography," Nanoscale Res Lett. **9**, 320 (2014).
101. T. Das Gupta, L. Martin-Monier, W. Yan, A. Le Bris, T. Nguyen-Dang, A. Gérald Page, K.-T. Ho, F. Yesilköy, H. Altug, Y. Qu, and F. Sorin, "Self-assembly of nanostructured glass metasurfaces via templated fluid instabilities," Nat. Nanotechnol. **14**, 320–327 (2019).
102. M. Petrich, M. Stambke, and J. P. Bergmann, "Examinations on laser remote welding of ultra-thin metal foils under vacuum conditions," Phys. Procedia **56**, 768–775 (2014).
103. H. Ogawa, M. Yang, Y. Matsumoto, and W. Guo, "Welding of metallic foil with electron beam," J. Solid Mech. Mater. Eng. **3**, 647–655 (2009).
104. A. Few, T. Lockett, R. Wilson, D. Boling, and E. Loper, "Testing and maturing a mass translating mechanism for a deep space CUBESAT," in *Proceedings of the 44th Aerospace Mechanisms Symposium*, May 16–18, 2018 (NASA Glenn Research Center, 2018).
105. D. C. Ullery, S. Soleymani, A. Heaton, J. Orphee, L. Johnson, R. Sood, P. Kung, and S. M. Kim, "Strong solar radiation forces from anomalously reflecting metasurfaces for solar sail attitude control," Sci. Rep. **8**, 10026 (2018).
106. K. Achouri and C. Caloz, "Metasurface solar sail for flexible radiation pressure control," arXiv:1710.02837 (2017).
107. Y. J. L. Chu, N. V. Tabiryan, and G. A. Swartzlander, "Experimental verification of a bigrating beam rider," Phys. Rev. Lett. **123**, 244302 (2019).
108. Y. J. L. Chu, E. M. Jansson, and G. A. Swartzlander, "Measurements of radiation pressure owing to the grating momentum," Phys. Rev. Lett. **121**, 063903 (2018).
109. G. A. Swartzlander, "Radiation pressure on a diffractive sailcraft," J. Opt. Soc. Am. B **34**, C25–C30 (2017).
110. Y.-W. Huang, H. W. H. Lee, R. Sokhoyan, R. A. Pala, K. Thyagarajan, S. Han, D. P. Tsai, and H. A. Atwater, "Gate-tunable conducting oxide metasurfaces," Nano Lett. **16**, 5319–5325 (2016).
111. A. Howes, W. Wang, I. Kravchenko, and J. Valentine, "Dynamic transmission control based on all-dielectric Huygens metasurfaces," Optica **5**, 787–792 (2018).
112. S.-Q. Li, X. Xu, R. M. Veetil, V. Valuckas, R. Paniagua-Domínguez, and A. I. Kuznetsov, "Phase-only transmissive spatial light modulator based on tunable dielectric metasurface," Science **364**, 1087–1090 (2019).
113. A. Komar, R. Paniagua-Dominguez, A. Miroshnichenko, Y. F. Yu, Y. S. Kivshar, A. I. Kuznetsov, and D. Neshev, "Dynamic beam switching by liquid crystal tunable dielectric metasurfaces," ACS Photon. **5**, 1742–1748 (2018).
114. J. Murray, D. Ma, and J. N. Munday, "Electrically controllable light trapping for self-powered switchable solar windows," ACS Photon. **4**, 1–7 (2017).
115. N. Tabiryan, D. Roberts, D. Steeves, and B. Kimball, "4G optics: new technology extends limits to the extremes," in Photonics Spectra (March 2017), pp. 46–50.
116. D. Roberts, H. Xianyu, S. Nersisyan, N. V. Tabiryan, and E. Serabyn, "Overcoming the tradeoff between efficiency and bandwidth for vector vortex waveplates," in *IEEE Aerospace Conference*, Big Sky, Montana, USA (2019), pp. 1–15.
117. M. S. Venzmer and V. Bothmer, "Solar-wind predictions for the parker solar probe orbit," Astron. Astrophys. **611**, A36 (2018).
118. D. Rivera, R. E. Wirz, and N. M. Ghoniem, "Experimental measurements of surface damage and residual stresses in micro-engineered plasma facing materials," J. Nuclear Mater. **486**, 111–121 (2017).
119. Y. Hirooka, T. Imoto, and T. Sano, "Helium ion irradiation on chemically deposited molybdenum and molybdenum carbide," J. Nuclear Mater. **113**, 202–206 (1983).
120. T. R. Lockett, J. Castillo-Rogez, L. Johnson, J. Matus, J. Lightholder, A. Marinan, and A. Few, "Near-earth asteroid scout flight mission," IEEE Aerosp. Electron. Syst. Mag. **35**(3), 20–29 (2020).
121. S. Gong and M. Macdonald, "Review on solar sail technology," Astrodynamics **3**, 93–125 (2019).
122. S. Pellegrino, ed., *Deployable Structures* (Springer, 2014).
123. T. D. Ngo, A. Kashani, G. Imbalzano, K. T. Q. Nguyen, and D. Hui, "Additive manufacturing (3D printing): a review of materials, methods, applications and challenges," Composites, Part B **143**, 172–196 (2018).
124. S. Chand, "Review carbon fibers for composites," J. Mater. Sci. **35**, 1303–1313 (2000).

125. D. K. Rajak, D. D. Pagar, P. L. Menezes, and E. Linul, "Fiber-reinforced polymer composites: manufacturing, properties, and applications," Polymers **11**, 1667 (2019).
126. M. Wentzel-Long and G. A. Landis, "Power generation from interplanetary and interstellar plasma and magnetic fields," in *AIAA Propulsion and Energy 2020 Forum* (2020), paper AIAA 2020-3537.
127. A. J. Minnich, M. S. Dresselhaus, Z. F. Ren, and G. Chen, "Bulk nanostructured thermoelectric materials: current research and future prospects," Energy Environ. Sci. **2**, 466–479 (2009).
128. S. Twaha, J. Zhu, Y. Yan, and B. Li, "A comprehensive review of thermoelectric technology: materials, applications, modelling and performance improvement," Renew. Sustain. Energy Rev. **65**, 698 (2016).
129. D. G. Messerschmitt, P. Lubin, and I. Morrison, "Challenges in scientific data communication from low-mass interstellar probes," Astrophys. J. Suppl. Ser. **249**, 36 (2020).
130. A. Biswas, M. Srinivasan, R. Rogalin, S. Piazzolla, J. Liu, B. Schratz, A. Wong, E. Alerstam, M. Wright, W. Roberts, J. Kovalik, G. Ortiz, A. Na-Nakornpanom, M. Shaw, C. Okino, K. Andrews, M. Peng, D. Orozco, and W. Klipstein, "Status of NASA's deep space optical communication technology demonstration," in *IEEE International Conference on Space Optical Systems and Applications (ICSOS)*, Naha, Japan (2017), pp. 23–27.
131. W. Hart, G. M. Brown, S. M. Collins, M. De Soria-Santacruz Pich, P. Fieseler, D. Goebel, D. Marsh, D. Y. Oh, S. Snyder, N. Warner, G. Whiffen, L. Elkins-Tanton, J. Bell, D. J. Lawrence, P. Lord, and Z. Pirkl, "Overview of the spacecraft design for the Psyche mission concept," in *IEEE Aerospace Conference*, Big Sky, Montana, USA (2018), pp. 1–20.
132. C. Xiang, P. A. Morton, and J. E. Bowers, "Ultra-narrow linewidth laser based on a semiconductor gain chip and extended Si_3N_4 Bragg grating," Opt. Lett. **44**, 3825–3828 (2019).
133. G. Marx, "Interstellar vehicle propelled by terrestrial laser beam," Nature **211**, 22–23 (1966).
134. J. L. Redding, "Interstellar vehicle propelled by terrestrial laser beam," Nature **213**, 588 (1967).
135. W. E. Moeckel, "Propulsion by impinging laser beams," J. Spacecr. Rockets **9**, 12 (1972).
136. R. L. Forward, "Roundtrip interstellar travel using laser-pushed lightsails," J. Spacecr. Rockets **21**, 187–195 (1984).
137. G. A. Landis, "Optics and materials considerations for a laser-propelled lightsail," in *40th International Astronautical Congress*, Malaga, Spain (1989).
138. G. A. Landis, "Small laser-propelled interstellar probe," in *46th International Astronautical Congress*, Norway (1995).
139. G. A. Landis, "Dielectric films for solar and laser-pushed lightsails," AIP Conf. Proc. **504**, 989 (2000).